Biochimie 108 (2015) 33–39

Contents lists available at ScienceDirect

Biochimie

journal homepage: www.elsevier.com/locate/biochi

Research paper

Structural insight into the conformational change of alcohol dehydrogenase from *Arabidopsis thaliana* L. during coenzyme binding

FangFang Chen [1], Ping Wang [1], Yan An, JianQin Huang, YingWu Xu*

The Nurturing Station for the State Key Laboratory of Subtropical Sylviculture, Zhejiang Agriculture and Forestry University, Lin'an, Zhejiang 311300, China

ARTICLE INFO

Article history:
Received 12 June 2014
Accepted 26 October 2014
Available online 4 November 2014

Keywords:
Alcohol dehydrogenase
Crystal structures
Conformational change
Coenzyme binding

ABSTRACT

Alcohol dehydrogenase (ADH, EC 1.1.1.1) plays important roles in the metabolism of alcohols and aldehydes. They are often subjected to conformational changes that are critical for the enzymatic activity and have received intensive investigation for horse liver ADH. However, for the large plant ADH members, little is known regarding both the conformational change and its relationship to catalytic activity as plant ADH structures were rarely available. Here we describe three Arabidopsis ADH conformations obtained from two crystals, the apo crystal that was free of ligand, and the complex crystal that was with NAD. The NAD-complexed crystal yielded two different structural forms for the two subunits, one was occupied by the coenzyme, and the other was free and open. Structural comparisons demonstrate that the occupied subunit is in a closed conformation while the free subunit is fully open, and the apo structure in intermediate. Though all the forms have an overall fold similar to that of horse and human ADHs, the catalytic domain has an over 10° rotation. Additionally, unlike horse liver ADH, the loop (295–302aa) adopts different conformation. It does not rearrange upon the binding of the coenzyme norVal297 side chain experiences a flipping. Instead it always remains in the active site. His48 plays a switching role in the structure. Its imidazole ring has to swim away from the binding site to permit NAD binding. These together with the large differences in the substrate binding pocket, as well as in the proton relay system demonstrate that AtADH adopts a different catalysis mechanism from horse liver ADH.

1. Introduction

Alcohol dehydrogenase (ADH, EC 1.1.1.1) belongs to the medium-chain dehydrogenases/reductases superfamily whose activity has been reported in all types of organisms [1,2]. The representative member is the horse liver ADH (HLADH) consisting of two sequence identical subunits composed of a catalytic domain and a coenzyme binding domain (BD). Crystal structural analysis has demonstrated that upon binding of NAD or NADH, the domains are subjected to conformational changes which play an important role for the catalysis [3–5]. For HLADH, these changes mainly involve the catalytic domain rotation around an axis between the catalytic domain and the coenzyme BD, and the loop (residues 293–299) rearrangement involving a Valine side chain flipping.

Plants have a large number of ADH members which play important roles in fruit ripening and seedling, in response to environmental stresses and the ABA phytohormone [6,7]. The single copy of ADH in *Arabidopsis thaliana* is essential for the survival of plants during anaerobic conditions [8]. Plant ADHs have been investigated mainly through phylogeny, which suggested the existence of multiple copies of ADHs in different plants except Arabidopsis [9]. Thompson et al. attempted to connect ADH evolution to 3D structures [10]. However, due to lack of crystal structure for plant ADH, homolog modeling tools were used to build ADH 3D structures which formed the structural bases to analyze the functional divergence and molecular evolution among several plant ADHs. Similar method had been used to map plant 3D model base on horse ADH structures for the analysis of genetic diversification within the ADH gene family [9]. Obviously, accurate 3D structures are essential for these types of studies and demand to be experimentally determined. However, plant ADHs, such as rice and Arabidopsis ADHs, are significantly different from the widely studied human and horse ADHs with a homology around 51% or below. The combination of this low homology, domain conformational changes and the variations of sequence forming ligand pockets make the prediction of structural details speculative. Furthermore, it is unknown how flexible the plant ADHs would be, and how it is

* Corresponding author. Tel.: +86 571 6374 1673; fax: +86 571 6373 2738.
E-mail address: yxu@zafu.edu.cn (Y. Xu).
[1] These authors contributed equally to this work.

http://dx.doi.org/10.1016/j.biochi.2014.10.023
0300-9084/

related to the different catalytic properties compared with yeast and horse ADHs [11].

Here we report three AtADH structures obtained from two independent crystals. One crystal is free of ligand leading to apo form structure. The other is cocrystallized with coenzyme NAD leading to two different forms for the two subunits, one occupied by the coenzyme and the other free. The conformations are compared together with ADHs from other species. The 3D structural characteristic, ligand binding sites and proton relay mechanism are described and analyzed. The results revealed that AtADH share some common traits with other ADHs but has its own distinct features.

2. Materials and methods

2.1. Protein expression, purification, and crystallization

The AtADH gene (accession number P06525) encoding residues from 6 to 379 was subcloned into pET28a vector that was modified to harbor a tobacco etch virus (TEV) protease restriction sequence between thrombin and BamHI sites. The protein was expressed in BL21(DE3) cells and induced by 0.2 mM IPTG over night at 20 °C with a shaking speed of 220 rpm. Cells were harvested next morning and stored frozen at −80 °C.

The His-tagged AtADH was purified on nickel resin, eluted with 200 mM Imidazole, cleaved with TEV protease. The free AtADH was further cleared by size exclusion chromatography. The protein was concentrated to 40 mg/ml in the storage buffer containing 100 mM NaCl and 20 mM TrisHCl, pH 7.5. Mutation Tyr52 to His was performed according the QuickChange method. Its expression, purification and activity measurement are same as the wild type enzyme [11].

For crystallization, the protein was diluted down to 5 mg/ml in the storage buffer. Crystals were obtained at 22 °C in hanging drops using 2.0 M ammonium sulfate, 0.1 M acetate pH 5.9, and 1% glycerol as a precipitant. The crystals belong to hexagonal space group $P6_122$ with unit cell dimensions of $a = b = 103.6$ Å, $c = 168.1$ Å. The asymmetric subunit contains a single ADH polypeptide chain. The complex crystals were obtained in the presence of 40 mM NAD with a reservoir condition containing 15% (w/v) PEG-3350, 0.1 M acetate pH 4.8. This in fact yielded a neutral pH environment for the crystal as NAD was prepared in alkaline buffer. The produced crystals have unit cell dimensions $a = b = 101.2$ Å, $c = 165.7$ Å, slightly smaller than these for the apo crystals. The complex crystal behaved a twin property, and the diffraction data were processed in the trigonal space system $P3_121$, a sub-space group of $P6_122$ with a dimer in the asymmetric unit.

2.2. X-ray diffraction data collection and processing

X-ray diffraction data of the enzyme along were collected from a flash-cooled crystal at 100 K using a Rigaku R-AXIS VII++ image plate detector with CuKα radiation from rotating anode generators, Rigaku FR-E+ SuperBright (Rigaku Corporation, Tokyo, Japan). Crystals were flash frozen in a cryoprotectant containing 2.8 M ammonium sulfate, 15%glycerol, and 0.1 M acetate pH 5.9. 212 frames over 106° rotation were collected and processed using HKL3000 [12] to 2.30 Å resolution with an R-merge of 0.085 for all the reflections.

The diffraction data of the complex crystals were collected at synchrotron radiation on beamline BL17U of SSRF, Shanghai, China at 2.5 Å resolution. The crystals were cryo-protected in 35% PEG3350 and 0.1 M acetate pH 4.8. The diffraction data was then processed using the software program iMosflm [13] and the individual frames were merged together using the program SCALEPACK [14] with an R-merge of 0.11 for all reflections. The amplitudes were computed from intensities using the program TRUNCATE [15] in the CCP4 suite [16].

2.3. Structure determination and refinement

The substrate free enzyme structure was solved by molecular replacement using the program MOLREP [17] from CCP4 suite. The initial model was the single peptide chain of human glutathione-dependent formaldehyde dehydrogenase (PDB code: 2fzw) which shares 53% identity with AtADH. After the orientation and the translation were validated by the electron density map, the initial model sequence was mutated to AtADH in Coot [18] based on the sequence alignment. This model was further rebuilt using Coot and refined using the refinement module in Phenix [19]. The final model contains 375 continuous amino acids, including the first serine residue introduced by the cloning, two Zincs, four sulfates, and 185 waters.

The diffraction data on the NAD complex was initially integrated in the point group 622. The crystal has similar cell dimensions and same space group $P6_122$ as the NAD-free crystal. But further refinement stops the R_{free}/R values at 0.32/0.27. The reflection data were then examined by the program Xtriage [20] and revealed to be twin with a twin fraction of 47.8% and an operator of $(-h, -k, l)$. The 2.5 Å data set was then reindexed and the space group was determined by molecular replacement to be $P3_121$, under which there are two polypeptide chains in the asymmetric unit. The consecutive refinement was performed in the presence of twin law and the main chain dihedrals were restrained to the free enzyme structure. After an initial round of refinement, one of the two subunits was found to show extra electron density fitting NAD structure that was then modeled into the map, and included in the following refinement. The X-ray diffraction data and the refinement statistics are summarized in Table 1.

3. Results and discussion

3.1. Apo AtADH structure

3.1.1. Overall structure

The final model structure shows a good overall quality as evidenced by the statistics presented in Table 1. There are no residues in the disallowed regions of the Ramachandran plot except Cys177 which falls in the generously allowed region. The equivalent cysteine residue in human and HLADHs is also observed in the similar configuration [21,22]. Cys177, together with Cys47, His69 and an acetate anion are found to coordinate with the catalytic Zinc ion (Fig. 1A). The structural Zinc ion is associated with Cys47, Cys99, Cys102 and Cys105. Both Zincs are at the center of the tetrahedron.

The main chain conformation has an overall similarity with the mammal enzymes (Fig. 1B) in spite of many sequence differences (Fig. 1S). Superimposing AtADH subunit with human ADH or HLADH gave a root mean square derivation (RMSD) in the range of 1.4–1.6 Å for all the Cα atoms (Table 2). Similar to many reported ADH crystal structures [4], AtADH contains a catalytic domain mainly consisting of antiparallel pleated-sheets and a coenzyme binding domain (BD, 178–326aa) with a typical Rossmann fold for nucleotide binding. The conformations of coenzyme BDs are much more conserved relative to the catalytic domains. Arabidopsis and horse coenzyme BDs are superimposed with an RMSD value of 0.75 Å, half of the RMSD value of the full length, while the catalytic domains are superimposed with an RMSD value of 3.5 Å, twice of the RMSD value of the full length.

3.1.2. Dimer interface

AtADH has been shown to be a dimer in solution like mammalian and other alcohol dehydrogenases [11]. The dimer,

which has crystallographic symmetry in the apo form (Fig. 2A), contains an extensive subunit interface with a buried area of 3350 Å^2, 20 hydrogen bonds and 14 salt bridges when evaluated by the protein interface software PISA [23] (Fig. 2B). The contact surface is composed by residues mainly from two patches. One patch contains residues from 103 to 112 which are stabilized by the conserved structural Zinc. It contributes about 20% of the buried area. The other patch contains residues from 286 to 324 which contribute about 77% of the buried area and form a conserved contact interface typically observed for ADH from many other species [4]. In this region, residues from 302 to 321 form a βαβ (β15α9β16) motif that packs with the same residues from the other subunit and extends the β-sheet of the catalytic domain into a larger sheet element (Fig. 2A). The two pairs of the beta sheets contribute 8 pairs of hydrogen bonds in stabilizing the dimer. It is worth to point out that at this region, there is no need for the residues to be conserved to form the conserved interface since the contacts involve the main chain hydrogen bonds between the antiparallel β strands (β15–β15′ and β16–β16′) between the subunits. In fact, when compared with HLADH, AtADH has only 8 amino acids similar among the 20, corresponding to 40% similarity, much lower than the overall similarity of 68%. Other plants, such as rice and maize share high sequence identity with Arabidopsis in this region should form dimer using the same mechanism though they have lower sequence similarity compared with horse or human counterparts.

3.2. AtADH–NAD complex structure

3.2.1. Overall structure

Unlike the apoenzyme structure, the asymmetric subunit of the NAD complexed structure contains a dimer. However, only one subunit (B) is occupied by the coenzyme that is located in the expected binding pocket formed by the coenzyme BD and the catalytic domain (Fig. 3A and B). Lack of NAD in subunit A may be not due to crystal packing as the two subunits have similar environments due to the existence of a crystallographic pseudo-rotational 2-fold axis between the two subunits, and there is no any residue nearby to block NAD entering to its binding sites, which face very wide tunnels in the crystal.

The binding site is seated between the two domains to the Nicotinamide side. Overall, both subunits A and B are similar to the apoenzyme structure in the main chain conformation. Their superposition yielded overall RMSD values of 0.7–1.0 Å for all the 375 α-carbons (Table 2). However, the overlapping of the subunit A with B within the dimer showed a larger difference of 1.48 Å, indicating that binding of NAD caused a large conformation change within the dimer. Indeed, relative to the subunit A, coenzyme binding induces the catalytic domain a 12.6° closure rotation when analyzed by Dyndom [24] (Fig. 3C). This rotation has only 5.5° when referenced to the Apo enzyme. For the loop 56–60aa at the very top of the binding pocket (Fig. 3C), above rotation respectively corresponds to up to 5.0 Å and 2.5 Å translations.

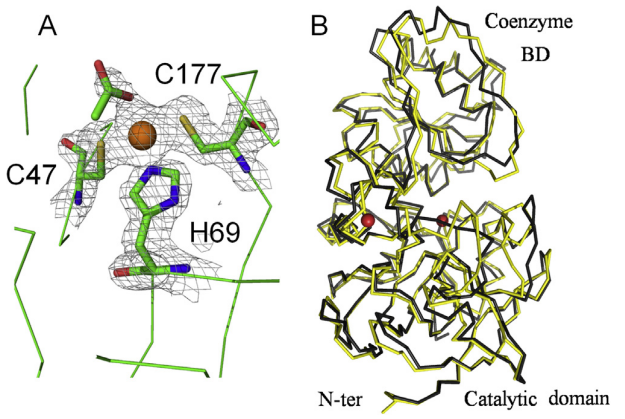

Fig. 1. A. 2Fo–Fc electron density map countered at 2sigma around the catalytic Zinc ion together with the coordinated residues Cys177, Cys47, His69, and an acetate anion. Residues are shown in sticks with color codes: red for oxygen, blue for nitrogen, yellow for sulfur, and green for carbon. All Zincs are shown in red balls. B. The main chain superimposing of AtADH with HLADH shows an overall similarity between the two apo form structures. AtADH is in black ribbon and HLADH in yellow. The lower part is the catalytic domain and the upper part the coenzyme BD. All figures are made in PyMol [35].

Table 1
X-ray data collection and refinement statistics.

Data collection statistics		
Crystal	ADH	ADH–NAD
Wavelength (Å)	1.5418	0.979
Cell dimension $a = b$, c (Å)	103.6, 168.1	101.2, 165.6
Space group	$P6_122$	$P3_121$
Resolution (Å)	2.3 (2.37–2.3)	2.5 (2.64–2.5)
Unique reflections	24,387	33,370(4043)
Completeness (%)	99.9(99.9)	96.8(82.9)
Redundancy	12.2(12.2)	3.7(1.5)
Average I/sigma	22.3(5.8)	9.9(2.3)
R_{merge}	0.076(0.513)	0.11(0.298)
Refinement statistics		
Reflections	24,362	33,347
Twin law		$-h, -k, l$
Twin fraction		0.478
Number of protein atoms	2863	5726
Number of Zn	2	4
Number of NAD atoms	0	44
Number of waters	185	57
R_{cryst}/R_{free} (%)	16.2/20.0	15.2/18.3
Average B-factor (Å^2)	33.5	37.2
Bond lengths (Å)	0.005	0.019
Bond angles (°)	0.838	1.76

Values in parentheses correspond to highest resolution shell.
$R_{merge} = \sum_{hkl}|I(hkl) - \langle I(hkl)\rangle| / \sum_{hkl} I(hkl)$ where $I(hkl)$ is the measured intensity of the reflections with indices *hkl*.
R_{free} values were calculated with 7.3% of the reflections that were excluded from the refinement.

3.2.2. Coenzyme binding pocket

NAD binding mode in Arabidopsis is essentially the same as horse holoenzyme, both are in a closed conformation. The adenine base is positioned in a hydrophobic cleft with the nicotinamide heading to the active site cleft. To illustrate the differences, Fig. 4A shows the main contact residues that are different in Arabidopsis and horse. The snapshot is taken from His48 toward the coenzyme BD. The elements from horse are shown in thin lines, from Arabidopsis in thick sticks. The NADs are found almost in the same position and orientation except the adenine rings, whose surfaces

Table 2
RMSD comparisons between different ADHs.

	At-free	At-NAD	Human-NAD	Horse-NAD	Horse-Apo
At-Apo	0.67	1.01	1.56 (49.6%)	1.38 (51.5%)	1.41
At-free		1.48	1.83	2.00	1.56
At-NAD			1.01	1.05	1.41

RMSD values (Å) were obtained by overlaying the secondary structures of the corresponding Arabidopsis subunits onto the NAD bound and the apo forms of the enzymes. The superposition was performed in Coot over all the residues. PDB codes used are: Human-NAD: 1HSO (NAD complex); Horse-NAD: 2OHX (NAD complex); Horse-Apo: 1YE3 (Apo enzyme). The sequence identity between AtADH and the corresponding ADH is included in the parentheses.

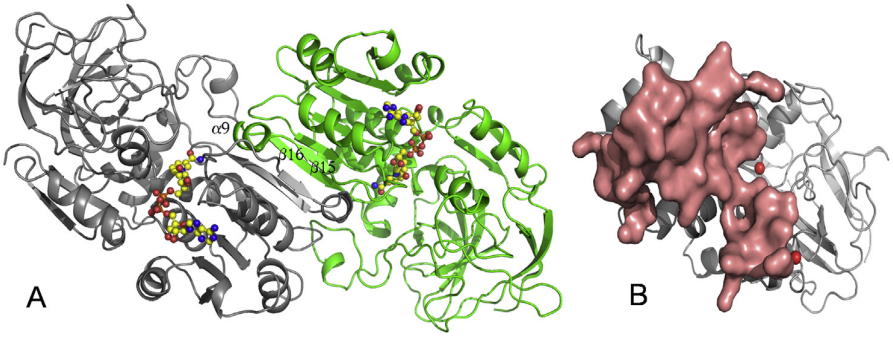

Fig. 2. Illustration of the quaternary structure arrangement for the functional AtADH dimer. A. The protein is shown in ribbon diagram and colored in gray and green for the subunits, respectively. The ball-stick NAD molecules are docked to highlight the potential binding positions. B. The subunit contact region is displayed with salmon surface. Zincs are shown in red balls. The catalytic Zn is in the middle and the structural Zn in the bottom. The remaining part of the protein is shown in ribbon diagram.

form a 10° of angle. Adenine ring is clamped between Ile270 and Ile225 in HLADH with the side chain of Arg273 over the head of the ring. The two hydrophobic residues are replaced by Ser274 and Phe227 in AtADH. This replacement pushes adenine ring toward to the coenzyme BD in Arabidopsis. The hydrogen bond formed between Lys229 and adenosine ribose is maintained through Arg231 in Arabidopsis. A major interaction difference between the two enzymes is that Arg48 and His52 in horse are replaced by His48 and Tyr52 in Arabidopsis (Fig. 5). His48 conformation in the NAD bound state is found different from apo or open states, in which its imidazole ring points to the coenzyme binding pocket. It has to swing out of the site to avoid the clashing with the incoming coenzyme. The equivalent position is Arg48 in horse. In its apo form, Arg48 takes the similar conformation as in NAD bound state; therefore it has no need to alter its conformation for NAD binding. This may be part of the reason that NAD binds horse enzyme with a higher affinity (0.026 mM) than Arabidopsis counterpart (1.6 mM) [11].

3.2.3. Substrate binding pocket

An overall view of the substrate binding pocket is displayed in Fig. 4B, where horse enzyme is included as comparison. The inner part of the substrate pocket is much conserved and is composed of Thr49, Phe95, Phe143, and Leu144 (not shown in the figure). Threonine at position 49 is conserved in plants but it is serine in horse and human (Fig. 1S). The extra methyl group in threonine side chain points to the substrate binding pocket and has an negative impact on the activity for secondary alcohol [25]. Indeed, isopropanol has about one fifth activity of ethanol for AtADH, while the short primary alcohols are almost equal active as ethanol [11].

In contrast to the inner part, the pocket outer part is most variable in ADH family. It is mainly composed by loops that are addressed in Fig. 4B. Based on sequence alignment, three pairs of residues at the equivalent positions are shown to highlight the variations. Loops 57–63 and 117–124 are in the catalytic domain. Relative to HLADH, they have one residue insertion that may be partly responsible for the large movements. As shown in the figure, Pro61 from the two proteins are separated as far as 6 Å and the proline rings point to opposite directions. Similarly, Thr120 in the loop 117–124, is about 7 Å away from its equivalent horse residue Met119. Additionally, Thr120 side chain points to the inside of the pocket while Met119 to the outside. In the coenzyme BD, loop 298–302 contributes partly to the formation of the substrate binding pocket. Compared with HLADH, this loop has a large movement too. The equivalent residues Lys300 and Asp298 carry opposite charge, and point to opposite directions. This loop conformation itself adjusts significantly in horse upon the coenzyme binding, but not in AtADH. These comparisons indicate that substrate binding pockets are quite different between horse and Arabidopsis enzymes. It is possible that these differences differentiate the substrate activity as AtADH is obviously less active than HLADH [11].

3.2.4. Proton relay mechanism

The proton relay mechanism has been often proposed for HLADH through alcohol oxygen to Ser49 side chain oxygen, then to O2′ of the ribose on Nicotinamide side, which is further hydrogen bonded to His52 as illustrated in Fig. 5A [26]. Recent atomic resolution structures of HLADH further support this principle [27]. However, Arabidopsis can not take the same scheme due to lack of Ser-His system on the similar position (Fig. 5B). Though Thr49 can replace Ser49 with its side chain oxygen bridging the alcohol oxygen (a

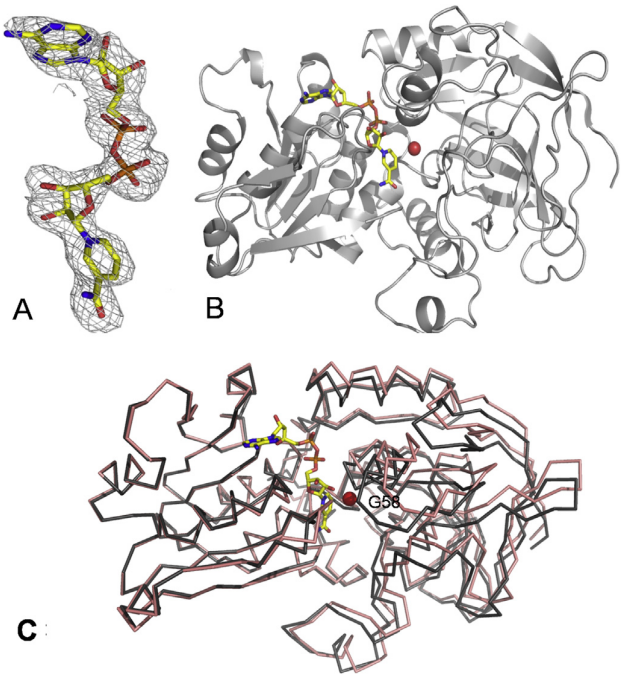

Fig. 3. A. Fo–Fc electron density map countered at 2.5sigma around the NAD. The map was calculated after a simulation annealing refinement during which the coenzyme was omitted. B. NAD in the binding site. The enzyme main chain conformation is shown in gray carton. C. Comparison of the NAD-bound subunit with the apo AtADH structure. The conserved coenzyme BDs were superimposed together. NAD-bound subunit is in black, Apo form in salmon. All NADs are shown in sticks.

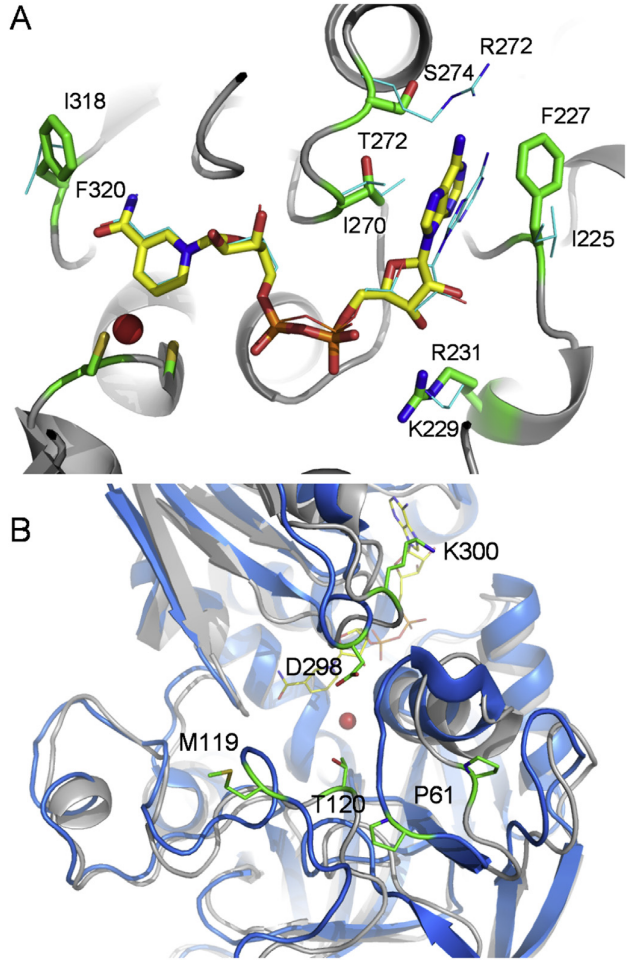

Fig. 4. A. The main NAD contact residues different in Arabidopsis and Horse. The snapshot is taken from His48 toward the coenzyme BD. The elements from Arabidopsis are shown in thick sticks, Horse in thin lines. B. An overall view of the substrate binding pocket. The AtADH is shown in light gray and Horse in marine. The large differences between the two enzymes are addressed by showing three pairs of residues at the equivalent positions.

water molecule in current structure) to the O2′, Tyr52 can not replace His52. Instead, the side chain of Tyr52 swings away from the ribose to the substrate active site. The nearby His48 can not replace His52 either as it can not form hydrogen bond with the ribose. This story is identical to cod ADH as shown in Fig. 5C, where there is a water molecule in the horse His52 position to form a hydrogen bond with O2′ [25]. Yet, this water molecule is not hydrogen bonded to His48, suggesting a direct proton dispatch to His48 is impossible and alternative pathway exists. Mutagenesis studies in HLADH suggested that His52 participates in, but is not essential for, proton transfers. His52 to Gln mutation retains the kinetic constants but shifts the pH dependencies for steady-state and transient reactions [28]. Contradictory results, however, were found for yeast and human enzymes, where the equivalent mutations significantly reduced the activity [29,30]. In our case, although mutation Tyr52 to His did not change coenzyme affinity apparently with Km = 0.74 ± 0.6 mM vs. 1.65 ± 0.4 mM for wild type, it increased the enzymatic activity about five fold with k_{cat} = 1550 ± 960 min^{-1} vs. 328 ± 107 min^{-1} for wild type [11]. It is possible that proton relay mechanism has multiple pathways and is species dependent.

3.3. Conformational changes

3.3.1. Comparison of domain conformations between AtADH and HLADH

Despite a large difference in the catalytic domains, Arabidopsis and horse apoenzymes have very similar openness for the coenzyme binding pockets (Fig. 1B), suggesting that they both are in the same conformational state. However, when the domain relative orientation was inspected, one found that the Arabidopsis catalytic domain has a 12° twist rotation relative to the same domain of horse apoenzyme after the coenzyme BDs are overlapped (Fig. 6A). The rotation occurs roughly around the β5 strand of residues from 89 to 93 (south–north direction in Fig. 6A). Structural wise, the catalytic domain is connected to coenzyme DB through linkers 176SCG and 321FFGNYKP (Fig. 1S). Both linkers contain a glycine residue that increases the linker flexibility. This may facilitate the relative movement between the two domains and contribute to coenzyme binding and catalytic activity. The linkers for human and HLADHs are even more flexible; they have two glycine residues (174GCG and 319FGGFKS). It is possible that existence of Glycine residues next to Cys177 may allow it a precise positioning for the catalytic Zinc (Fig. 1A) to achieve an efficient catalysis.

Unlike Apo ADHs, the domain orientations of NAD bound subunit are much more similar between Arabidopsis and horse. As

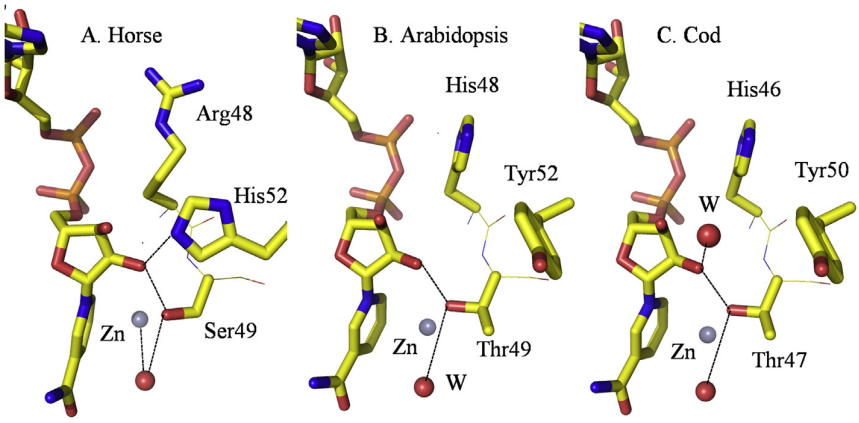

Fig. 5. Comparison of the proton relay systems among A. Horse; B. Arabidopsis; and C. Cod. All NADs and residues are shown in sticks, Zincs in gray balls and water in red balls. Dash lines stand for the hydrogen bonds.

shown in Fig. 6B, the catalytic domains do not experience an obvious twisting at all. This result suggests that AtADH conducts domain rotation through a different pathway from HLADH during coenzyme cycling.

3.3.2. Open, intermediate and closed forms of AtADH

Many ADH enzymes were crystallized with or without coenzyme. The complex crystal structures were often found with both sites occupied with NAD and generally called the closed form, with open form referring to the Apo enzyme. In this report, three structural forms for AtADH were found from two crystals with the NAD-complexed crystal containing two different forms. Comparison of the overall conformational differences is presented in Fig. 7, in which the coenzyme BDs are superimposed together. As seen in the figure, the catalytic domain is subjected to a rotation. The NAD-bound subunit takes the closed conformation, while the NAD-free subunit takes the open conformation with the apo structure as an intermediate. Relative to the closed conformation, the catalytic domain rotates 12.6° and 5.5° respectively. To our knowledge, this is first time that a set of three conformations was reported for any single type of ADH. Horse apoenzyme has the same opening as apo AtADH (Fig. 1B), suggesting that it may be an intermediate state too though the fully open conformation is never reported.

Early assays proposed a 'half-of-the-sites' mechanism for HLADH even though some researchers disagreed [31,32]. Whether current asymmetric dimer model supports this negative cooperativity between the two subunits still remains to be confirmed by kinetic measurements.

However, asymmetric conformation structure is not unique for AtADH. Yeast ADH–NAD complex structure is another example [33]. The opening of the NAD free and bound subunits is highly similar to AtADH–NAD structure when the corresponding subunits are superimposed respectively even though the two enzymes share only 20% sequence identity, supporting the perspective that ADHs have open, intermediate and closed conformations during the catalytic cycles.

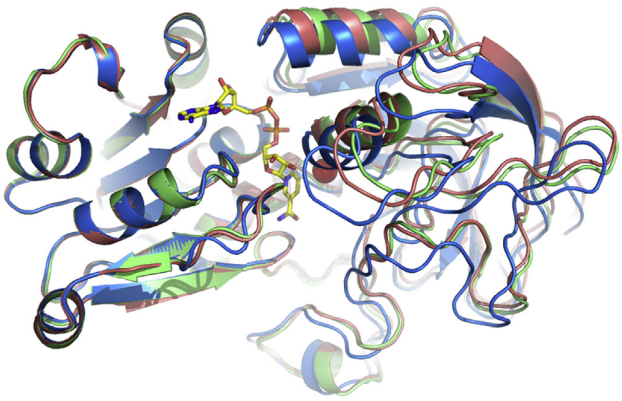

Fig. 7. Comparison of the three structural conformations for AtADH. The conserved coenzyme BDs were superimposed together. The intermediate state Apo form is colored in salmon, the open state NAD-free subunit in lime and the closed NAD-bound subunit in marine.

It is a common event that the catalytic domain undergoing a rotation upon binding of coenzyme. In HLADH, the rotation requires Val295 side chain flipping out from a buried position into the active site, which causes the loop (293–300aa) rearrangement and stabilizes it in the closed status [34]. However, this Valine (Val297) flipping story does not seem needed for AtADH though the amino acid is conserved between plants and horse. For the three AtADH forms, Val297 side chain constantly remains inside the active site and favors NAD binding, further demonstrating that AtADH adopts a different domain closing mechanism for coenzyme binding.

4. Conclusions

Closed, intermediate and open structural conformations have been obtained from two crystals. They represent three forms

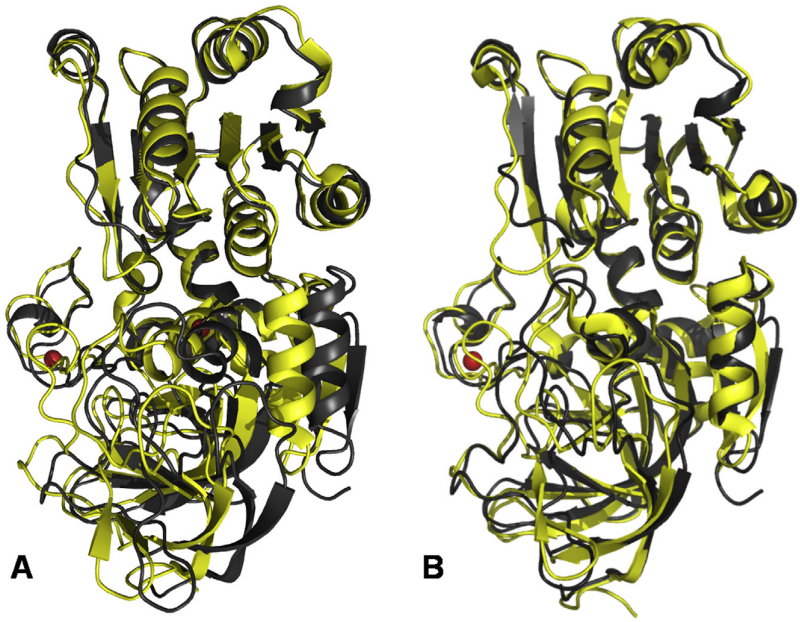

Fig. 6. Comparison of the overall conformational change between AtADH and HLADH after the coenzyme DBs are overlapped. A. The catalytic domain of Apo AtADH has a 12° twist rotation (to the right in the figure) relative to that of Apo HLADH. B. The closed form catalytic domain of AtADH has no twist rotation relative to that of HLADH. The main chains are shown in carton with black for AtADH and yellow for HLADH.

during the coenzyme cycling process. The major changes among them are the catalytic domain closure rotation and the switching of His48 imidazole ring. However, although AtADH hold similar fold and oligomeric arrangement as ADHs from other species, large differences are observed. Compared with HLADH, the domain closure rotation pathway is different. The catalytic domains of Apo AtADH and Apo HLADH have an angle of 12° but they end up almost perfectly overlapped in the middle upon NAD association. The loop (295–302aa) adopts different conformation too. It does not rearrange upon the binding of the coenzyme with Val297 side chain constantly remaining in the active site. Dramatic changes with movement of main chains and flipping of side chains have been observed for the residues forming the substrate binding site pocket. The proton relay system is different from HLADH but similar to Cod ADH. These results together demonstrate that AtADH adopts quite different catalysis mechanism from HLADH. In addition, current AtADH structures provided appropriate starting models to build 3D structures for various plant ADHs.

Funding

This work was supported by the National Natural Science Foundation of China (Grant No. 31270715), the 973 Initiation Project from The Ministry of Science and Technology of China (Grant No. 2011CB111500) and the Foundation from Zhejiang Agriculture and Forestry University (Grant No. 2010FR072).

Conflict of interest

The authors declare that there are no conflicts of interest.

Acknowledgments

The authors would like to thank Dr. Zhijun Zhang, the staffs from SSRF BL17U (Shanghai) and the crystallographic group of Biortus Corporation (Wuxi, China) for help with X-ray diffraction data collections. The refined crystallographic coordinates for AtADH and AtADH–NAD complex have been deposited in the Protein Data Bank with a designated accession codes 4RQT and 4RQU.

Appendix A. Supplementary data

Supplementary data related to this article can be found at http://dx.doi.org/10.1016/j.biochi.2014.10.023.

References

[1] B. Persson, J. Hedlund, H. Jornvall, Medium- and short-chain dehydrogenase/reductase gene and protein families : the MDR superfamily, Cell. Mol. Life Sci. 65 (2008) 3879–3894.
[2] C. Chang, E.M. Meyerowitz, Molecular cloning and DNA sequence of the *Arabidopsis thaliana* alcohol dehydrogenase gene, Proc. Natl. Acad. Sci. U. S. A. 83 (1986) 1408–1412.
[3] H. Eklund, J.P. Samma, L. Wallen, C.I. Branden, A. Akeson, T.A. Jones, Structure of a triclinic ternary complex of horse liver alcohol dehydrogenase at 2.9 A resolution, J. Mol. Biol. 146 (1981) 561–587.
[4] H. Eklund, S. Ramaswamy, Medium- and short-chain dehydrogenase/reductase gene and protein families: three-dimensional structures of MDR alcohol dehydrogenases, Cell. Mol. Life Sci. 65 (2008) 3907–3917.
[5] B.V. Plapp, Conformational changes and catalysis by alcohol dehydrogenase, Arch. Biochem. Biophys. (2010) 3–12.
[6] R. Dolferus, M. Jacobs, W.J. Peacock, E.S. Dennis, Differential interactions of promoter elements in stress responses of the Arabidopsis Adh gene, Plant Physiol. 105 (1994) 1075–1087.
[7] M. Zhang, S. Nagata, K. Miyazawa, H. Kikuchi, Y. Esashi, A competitive enzyme-linked immunosorbent assay to quantify acetaldehyde-protein adducts that accumulate in dry seeds during aging, Plant Physiol. 113 (1997) 397–402.
[8] J.R. Johnson, B.G. Cobb, M.C. Drew, Hypoxic induction of anoxia tolerance in roots of Adh1 null *Zea mays* L. Plant Physiol. 105 (1994) 61–67.
[9] B.S. Gaut, A.S. Peek, B.R. Morton, M.T. Clegg, Patterns of genetic diversification within the Adh gene family in the grasses (Poaceae), Mol. Biol. Evol. 16 (1999) 1086–1097.
[10] C.E. Thompson, C.L. Fernandes, O.N. de Souza, L.B. de Freitas, F.M. Salzano, Evaluation of the impact of functional diversification on Poaceae, Brassicaceae, Fabaceae, and Pinaceae alcohol dehydrogenase enzymes, J. Mol. Model. 16 (2010) 919–928.
[11] F. Cheng, T. Hu, Y. An, J. Huang, Y. Xu, Purification and enzymatic characterization of alcohol dehydrogenase from *Arabidopsis thaliana*, Protein Expr. Purif. 90 (2013) 74–77.
[12] W. Minor, M. Cymborowski, Z. Otwinowski, M. Chruszcz, HKL-3000: the integration of data reduction and structure solution–from diffraction images to an initial model in minutes, Acta Crystallogr. Sect. D Biol. Crystallogr. 62 (2006) 859–866.
[13] T.G. Battye, L. Kontogiannis, O. Johnson, H.R. Powell, A.G. Leslie, iMOSFLM: a new graphical interface for diffraction-image processing with MOSFLM, Acta Crystallogr. Sect. D Biol. Crystallogr. 67 (2011) 271–281.
[14] Z.M.W. Otwinowski, Processing of X-ray Diffraction Data Collected in Oscillation Mode, vol. 276, Academic Press, New York, 1997, pp. 307–326.
[15] J.E. Padilla, T.O. Yeates, A statistic for local intensity differences: robustness to anisotropy and pseudo-centering and utility for detecting twinning, Acta Crystallogr. Sect. D Biol. Crystallogr. 59 (2003) 1124–1130.
[16] CCP4, collaborative computational project, number 4, Acta Cryst. D50 (1994) 760–763.
[17] A. Vagin, A. Teplyakov, Molecular replacement with MOLREP, Acta Crystallogr. Sect. D Biol. Crystallogr. 66 (2010) 22–25.
[18] P. Emsley, K. Cowtan, Coot: model-building tools for molecular graphics, Acta Crystallogr. Sect. D Biol. Crystallogr. 60 (2004) 2126–2132.
[19] P.D. Adams, P.V. Afonine, G. Bunkoczi, V.B. Chen, I.W. Davis, N. Echols, J.J. Headd, L.W. Hung, G.J. Kapral, R.W. Grosse-Kunstleve, A.J. McCoy, N.W. Moriarty, R. Oeffner, R.J. Read, D.C. Richardson, J.S. Richardson, T.C. Terwilliger, P.H. Zwart, PHENIX: a comprehensive Python-based system for macromolecular structure solution, Acta Crystallogr. Sect. D Biol. Crystallogr. 66 (2010) 213–221.
[20] P. Zwart, R. Grosse-Kunstleve, P. Adams, CCP4 Newsletter 43, Contribution 7, 2005.
[21] S. Ramaswamy, H. Eklund, B.V. Plapp, Structures of horse liver alcohol dehydrogenase complexed with NAD+ and substituted benzyl alcohols, Biochemistry 33 (1994) 5230–5237.
[22] M.S. Niederhut, B.J. Gibbons, S. Perez-Miller, T.D. Hurley, Three-dimensional structures of the three human class I alcohol dehydrogenases, Protein Sci. 10 (2001) 697–706.
[23] E. Krissinel, K. Henrick, Inference of macromolecular assemblies from crystalline state, J. Mol. Biol. 372 (2007) 774–797.
[24] S. Hayward, H.J. Berendsen, Systematic analysis of domain motions in proteins from conformational change: new results on citrate synthase and T4 lysozyme, Proteins 30 (1998) 144–154.
[25] S. Ramaswamy, M. el Ahmad, O. Danielsson, H. Jornvall, H. Eklund, Crystal structure of cod liver class I alcohol dehydrogenase: substrate pocket and structurally variable segments, Protein Sci. 5 (1996) 663–671.
[26] H. Eklund, B.V. Plapp, J.P. Samama, C.I. Branden, Binding of substrate in a ternary complex of horse liver alcohol dehydrogenase, J. Biol. Chem. 257 (1982) 14349–14358.
[27] B.V. Plapp, S. Ramaswamy, Atomic-resolution structures of horse liver alcohol dehydrogenase with NAD(+) and fluoroalcohols define strained Michaelis complexes, Biochemistry 51 (2012) 4035–4048.
[28] L.A. LeBrun, D.H. Park, S. Ramaswamy, B.V. Plapp, Participation of histidine-51 in catalysis by horse liver alcohol dehydrogenase, Biochemistry 43 (2004) 3014–3026.
[29] T. Ehrig, T.D. Hurley, H.J. Edenberg, W.F. Bosron, General base catalysis in a glutamine for histidine mutant at position 51 of human liver alcohol dehydrogenase, Biochemistry 30 (1991) 1062–1068.
[30] B.V. Plapp, Site-directed mutagenesis: a tool for studying enzyme catalysis, Methods Enzymol. 249 (1995) 91–119.
[31] P. Andersson, G. Pettersson, Kinetic equivalence of the subunits of liver alcohol dehydrogenase, Eur. J. Biochem. 122 (1982) 559–568.
[32] J.T. McFarland, S.A. Bernhard, Catalytic steps during the single-turnover reduction of aldehydes by alcohol dehydrogenase, Biochemistry 11 (1972) 1486–1493.
[33] S. Ramaswamy, D.A. Kratzer, A.D. Hershey, P.H. Rogers, A. Arnone, H. Eklund, B.V. Plapp, Crystallization and preliminary crystallographic studies of *Saccharomyces cerevisiae* alcohol dehydrogenase I, J. Mol. Biol. 235 (1994) 777–779.
[34] S. Hayward, A. Kitao, Molecular dynamics simulations of NAD+-induced domain closure in horse liver alcohol dehydrogenase, Biophys. J. 91 (2006) 1823–1831.
[35] W.L. DeLano, The PyMOL User's Manual, DeLano Scientific, San Carlos, CA, USA, 2002.
[36] J.D. Thompson, T.J. Gibson, D.G. Higgins, Multiple sequence alignment using ClustalW and ClustalX, in: Andreas D. Baxevanis, et al. (Eds.), Current Protocols in Bioinformatics/Editorial Board, 2002 (Chapter 2), Unit 2.3.
[37] P. Gouet, X. Robert, E. Courcelle, ESPript/ENDscript: extracting and rendering sequence and 3D information from atomic structures of proteins, Nucleic Acids Res. 31 (2003) 3320–3323.